

Dyson-Schwinger approach to color superconductivity at finite temperature and density

D. Müller, M. Buballa, and J. Wambach

Institut für Kernphysik (Theoriezentrum), Technische Universität Darmstadt, Germany

(Dated: February 24, 2022)

We investigate the phases of dense QCD matter at finite temperature with Dyson-Schwinger equations for the quark propagator for $N_f = 2 + 1$ flavors. For the gluon propagator we take a fit to quenched lattice data and add quark-loop effects perturbatively in a hard-thermal-loop-hard-dense-loop approximation. We consider 2SC and CFL-like pairing with chiral up and down quarks and massive strange quarks and present results for the condensates and the phase diagram. We find a dominant CFL phase at chemical potentials larger than 500 – 600 MeV. At lower values of the chemical potential we find a 2SC phase, which also exists in a small band at higher temperatures for larger chemical potentials. With values of 20 – 30 MeV, the critical temperatures to the normal phase turn out to be quite small.

I. INTRODUCTION

The phase diagram of strong-interaction matter (QCD matter) is a central object in experimental and theoretical studies [1, 2]. At low temperatures and densities, quarks and gluons are confined into hadrons while at high temperatures free quarks and gluons are the dominant degrees of freedom.

The low-density regime of QCD matter is understood quite well as it is accessible by heavy-ion collisions and, on the theory side, by first-principles calculations on the lattice. These lattice QCD simulations at physical quark masses show a crossover transition from the hadronic phase at low temperatures to the quark-gluon plasma at high temperatures [3, 4].

On the other hand, the regime at non-vanishing net baryon densities is much less understood. Lattice QCD fails due to the fermion sign problem that prevents Monte Carlo simulations to be performed at non-zero baryon chemical potential, and only a small window can be accessed with extrapolation methods [5–9].

The regime of large densities and low temperatures is totally inaccessible with lattice QCD. There, quarks form Cooper pairs which condense as color superconductors [10–16]. At very high densities the coupling becomes small and QCD can be studied with weak-coupling methods. In this way, it was shown that the ground state is a color superconductor in the color-flavor-locked (CFL) phase, where up, down, and strange quarks are paired symmetrically [17–19]. On the other hand, at quark chemical potentials below 1 GeV, as relevant for the description of compact-star interiors, weak-coupling methods are not applicable, and one has to resort to non-perturbative methods. In this regime the strange-quark mass cannot be neglected against the chemical potential, eventually making the CFL pairing pattern unfavorable. This has been studied extensively in effective models, like the Nambu–Jona-Lasinio (NJL) model. It was found that at intermediate chemical potentials the 2SC phase is favored [20], in which only up and down quarks form Cooper pairs. Moreover, when the constraints of beta

equilibrium and electric neutrality are taken into account in addition, these model studies show a rich phase structure with many different types of color-superconducting condensates [21–23].

Unfortunately, these results are very sensitive to the model parameters. In order to make quantitative predictions, it is therefore necessary to employ non-perturbative methods which are directly rooted in QCD. In this context, Dyson-Schwinger equations (DSEs) are a promising approach. They have been used to investigate the chiral and deconfinement transition and good agreement with lattice results was obtained [24, 25]. In Refs. [26, 27], these studies were extended to finite density. It was found that the resulting phase diagram contains a critical endpoint beyond which the chiral phase transition becomes first-order.

Some time ago, the framework of DSEs was also applied to investigate color-superconducting phases at zero temperature [28–30]. In contrast to the NJL-model studies, these calculations showed that the CFL phase is the dominant phase down to rather low chemical potentials, leaving practically no room for other quark phases, like the 2SC phase.

In their exact formulation, DSEs are an infinite set of equations, which have to be truncated in practice. This should be done in a way that the most important features of QCD are included, while keeping the numerical effort on a reasonable level. Obviously, the truncated DSEs are no longer exact and typically require some model input for higher-order n -point functions. However, unlike effective models, they are applicable at all energy scales and the approximations are systematically amendable.

Recently, considerable progress was made in extracting some of the relevant input from the lattice. Specifically, there exists a temperature dependent parametrization of the quenched gluon propagator [25], which, together with a phenomenological ansatz for the quark-gluon vertex, has successfully been used as input for the DSE calculations of Ref. [26, 27]. Compared with earlier truncations, these gluon interactions turn out to be more attractive, leading to stronger non-perturbative effects.

One goal of the present paper is therefore to perform

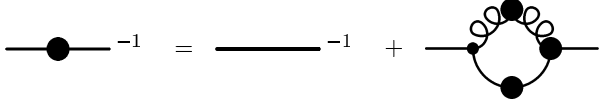


FIG. 1. Dyson-Schwinger Equation for the full quark propagator. Plain lines represent quark propagators, the curly line the gluon propagator. Thick dots represent dressed quantities.

an update of the DSE analysis of color-superconducting phases presented in Ref. [29], using this new, more realistic gluonic input. We will show that this changes the results qualitatively, making the existence of a 2SC phase at low temperatures possible. The second goal of this work is to extend these calculations to non-zero temperature, which was not studied in Ref. [29].

This paper is organized as follows. In sects. II and III, we introduce the quark DSEs and the structure of the quark propagators in a color superconducting environment. Our truncation scheme is presented in sect. IV. In sect. V, we discuss our results for the color-superconducting condensates and for the phase diagram. All calculations are performed for $N_f = 2 + 1$ flavors. Thereby, we restrict ourselves to the case of a flavor-independent chemical potential, postponing the analysis of electrically neutral matter to a later analysis. In sect. VI we discuss the phase diagram obtained with an alternative parametrization of the quark-gluon vertex and the gluon propagator, which leads to a better fit of vacuum quantities. Conclusion are drawn in sect. VII.

II. THE QUARK DYSON-SCHWINGER EQUATION

The dressed quark propagator $\mathcal{S}(p)$ is the solution of the Dyson-Schwinger equation (DSE)

$$\mathcal{S}^{-1}(p) = Z_2(\mathcal{S}_0^{-1}(p) + \Sigma(p)), \quad (1)$$

which is depicted diagrammatically in fig. 1. Here $p = (p_4, \vec{p})$ is the Euclidean 4-momentum. To describe the system at temperature T and chemical potential μ we use the Matsubara formalism, so that $p_4 = \omega_n + i\mu$ where $\omega_n = (2n + 1)\pi T$ are the fermionic Matsubara frequencies. $\mathcal{S}_0(p)$ denotes the bare quark propagator and Z_2 is the quark wave function renormalization constant.

The self-energy $\Sigma(p)$ is given by

$$Z_2 \Sigma(p) = g^2 \sum_q \Gamma_{\mu}^{a,0} \mathcal{S}(q) \Gamma_{\nu}^b(p, q) D_{\mu\nu}^{ab}(k = p - q) \quad (2)$$

with the dressed gluon propagator $D_{\mu\nu}^{ab}(k)$ and the bare and dressed quark-gluon vertices, $g\Gamma_{\nu}^{a,0}$ and $g\Gamma_{\nu}^b(p, q)$, respectively. a and b denote color indices, μ and ν Dirac indices and g represents the QCD coupling constant.

Furthermore, we have introduced the notation $\sum_q \equiv T \sum \int \frac{d^3 q}{(2\pi)^3}$, where the sum runs over the Matsubara frequencies corresponding to q_4 .

As we work in Landau gauge, the gluon propagator is transverse. In a thermal medium it can have two components in the transverse subspace,

$$D_{\mu\nu}^{ab}(k) = \frac{Z_{TT}^{ab}(k)}{k^2} P_{\mu\nu}^T(k) + \frac{Z_{TL}^{ab}(k)}{k^2} P_{\mu\nu}^L(k), \quad (3)$$

with the 3-dimensional transverse and longitudinal projectors

$$\begin{aligned} P_{\mu\nu}^T(k) &= \delta_{ij} - \frac{k_i k_j}{k^2}, \\ P_{\mu\nu}^L(k) &= T_{\mu\nu}(k) - P_{\mu\nu}^T(k) \end{aligned} \quad (4)$$

and the 4-dimensional transverse projector

$$T_{\mu\nu}(k) = \delta_{\mu\nu} - \frac{k_{\mu} k_{\nu}}{k^2}. \quad (5)$$

The gluon dressing functions $Z_{TT}^{ab}(k)$ and $Z_{TL}^{ab}(k)$ coincide in vacuum but, in general, differ in the medium, as the medium breaks the $O(4)$ symmetry of the vacuum.

The quark spinors are four-dimensional objects in Dirac space and have $3 \times N_f$ components in color-flavor space, where N_f is the number of flavors. In this article we generally consider $N_f = 3$, but sometimes refer to two-flavor systems for comparison. In addition we introduce the two-dimensional Nambu-Gorkov (NG) space, which easily allows to incorporate color superconductivity in the formalism [31, 32]. The NG spinors are defined by

$$\Psi = \frac{1}{\sqrt{2}} \begin{pmatrix} \psi \\ C \bar{\psi}^T \end{pmatrix}, \quad \bar{\Psi} = \frac{1}{\sqrt{2}} (\bar{\psi} \quad \psi^T C) \quad (6)$$

with the charge conjugation matrix $C = \gamma_2 \gamma_4$.

We take the conventions from [13, 28] and parametrize the propagators and self-energies in NG space as follows:

$$\mathcal{S}_0(p) = \begin{pmatrix} S_0^+(p) & 0 \\ 0 & S_0^-(p) \end{pmatrix} \quad (7)$$

$$\mathcal{S}(p) = \begin{pmatrix} S^+(p) & T^-(p) \\ T^+(p) & S^-(p) \end{pmatrix} \quad (8)$$

$$\Sigma(p) = \begin{pmatrix} \Sigma^+(p) & \Phi^-(p) \\ \Phi^+(p) & \Sigma^-(p) \end{pmatrix} \quad (9)$$

The components diagonal in NG space represent the normal propagators and self-energies for particles (+) and charge conjugate particles (−), while the off-diagonal components are related to color superconductivity. Therefore the bare propagator is diagonal in NG space. Without color superconductivity, also the

dressed propagator and the self-energy are diagonal, and the Dyson-Schwinger system decouples into two equivalent gap equations for the quark propagator and the charge conjugate propagator. On the other hand, if color-superconducting condensates are present, quarks and charge conjugate quarks are coupled.

This becomes evident when we insert the above expressions into the DSE, eq. (1). One then obtains the following set of equations, which are coupled through the color-superconducting condensates:

$$\begin{aligned} S^{\pm-1} &= Z_2 \left(S_0^{\pm-1} + \Sigma^\pm - \Phi^\mp (S_0^{\mp-1} + \Sigma^\mp)^{-1} \Phi^\pm \right) \\ T^\pm &= - (S_0^{\mp-1} + \Sigma^\mp)^{-1} \Phi^\pm S^\pm \end{aligned} \quad (10)$$

By construction, the two NG-spinors eq. (6) are not independent. As a consequence, the + and - components of the propagators are related to each other by

$$\begin{aligned} S^+(p) &= -CS^-(p)^T C, \\ T^+(p) &= -CT^-(p)^T C, \end{aligned} \quad (11)$$

$$\begin{aligned} S^+(p_4, \vec{p}) &= \gamma_4 S^+(-p_4, \vec{p})^\dagger \gamma_4, \\ T^+(p_4, \vec{p}) &= \gamma_4 T^+(-p_4, \vec{p})^\dagger \gamma_4, \end{aligned} \quad (12)$$

and analogously for the self-energies [13, 28].

The bare quark propagator is defined by

$$(S_0^+)^{-1}(p) = -i\not{p} + Z_m m_f \quad (13)$$

with the bare quark mass m_f and the mass renormalization constant Z_m for the quark flavor f . It follows that $(S_0^-)^{-1}$ takes the same form with μ replaced by $-\mu$.

The quark renormalization constants Z_2 and Z_m are determined by the renormalization condition in vacuum

$$S^{-1}(p^2 = \nu^2) = (-i\not{p} + m_f)|_{p^2=\nu^2} \quad (14)$$

at some arbitrary renormalization point ν .

The vertices also live in NG space. The bare vertex is diagonal

$$\Gamma_\mu^{a,0} = Z_{1F} \begin{pmatrix} \gamma_\mu \frac{\lambda_a}{2} & 0 \\ 0 & -\gamma_\mu \frac{\lambda_a^T}{2} \end{pmatrix} =: Z_{1F} \gamma_\mu \frac{\Lambda_a}{2}, \quad (15)$$

where λ_a are the 8 Gell-Mann matrices in color space. Z_{1F} is the renormalization constant of the quark-gluon vertex. The full vertex has off-diagonal elements in general,

$$\Gamma_\mu^a(p, q) = \begin{pmatrix} \Gamma_\mu^{a,+}(p, q) & \Delta_\mu^{a,-}(p, q) \\ \Delta_\mu^{a,+}(p, q) & \Gamma_\mu^{a,-}(p, q) \end{pmatrix}. \quad (16)$$

In this work, we only take into account the diagonal functions Γ^\pm which will be specified later, when we define our truncation scheme.

III. PARAMETRIZATION OF COLOR-SUPERCONDUCTING PHASES

In the following we restrict our calculations to spin-zero color-superconducting phases, which should be preferred over spin-one phases in most regions of the phase diagram. We are interested in the realistic case with two light quark flavors and a heavier strange quark. For simplicity, we consider massless up and down quarks but massive strange quarks. This corresponds to an intermediate situation between two idealized cases:

For infinitely heavy strange quarks, the strange sector decouples, and we are left with a two-flavor system. In this case, the 2SC phase is favored, where red and green up and down quarks form a diquark condensate, whereas blue quarks are not involved in the pairing. This leads to a breaking of the $SU_c(3)$ color symmetry to a $SU_c(2)$ subgroup, while the $SU_L(2) \otimes SU_R(2)$ chiral symmetry remains intact. The other extreme is to have three massless quark flavors. Here the favored phase is the CFL phase [17], where all colors and flavors participate in the pairing in a symmetric way, so that the $SU_c(3)$ color symmetry and the $SU_L(3) \otimes SU_R(3)$ chiral symmetry are broken down to a residual $SU_{c+V}(3)$ symmetry.

Turning on a finite but small strange-quark mass, a CFL-like phase can still be realized. In this phase all colors and flavors are paired in a diquark condensate, but there is only a residual $SU_{c+V}(2) \otimes U_{c+V}(1)$ symmetry, while the full CFL symmetry is only approximate. Alternatively there could be a 2SC phase, where the strange quarks remain unpaired.

In order to find the solutions of the DSE in a given color-superconducting phase, we follow Ref. [29] and expand the propagators and self-energies as

$$\begin{aligned} S^+(p) &= \sum_i S_i^+(p) P_i, \\ T^+(p) &= \sum_i T_i^+(p) M_i, \end{aligned} \quad (17)$$

and

$$\begin{aligned} \Sigma^+(p) &= \sum_i \Sigma_i^+(p) P_i, \\ \Phi^+(p) &= \sum_i \phi_i^+(p) M_i, \end{aligned} \quad (18)$$

with P_i and M_i being matrices color-flavor space. These matrices have been constructed such that they respect the symmetries of the considered phase and are complete in the sense that they yield a closed set of self-consistency equations when inserted into eq. (10). In the most general case, considered here, *i.e.*, the CFL-like phase with non-vanishing strange-quark mass, both sets, $\{P_i\}$ and $\{M_i\}$, consist of seven matrices, which are listed in Appendix A. More symmetric cases, such as the 2SC phase or non-superconducting phases, are contained in this parametrization as special limits, which are discussed in Appendix A as well.

The Dirac structure of the propagator is parametrized as [29, 33]

$$\begin{aligned}
S_i^{+-1}(p) &= \\
&-i(\omega_n + i\mu)\gamma_4 C_i^+(p) - i\vec{p}A_i^+(p) + B_i^+(p) - i\gamma_4 \frac{\vec{p}}{|\vec{p}|} D_i^+(p), \\
T_i^+(p) &= \\
&\left(\gamma_4 \frac{\vec{p}}{|\vec{p}|} T_{A,i}^+(p) + \gamma_4 T_{B,i}^+(p) + T_{C,i}^+(p) + \frac{\vec{p}}{|\vec{p}|} T_{D,i}^+(p) \right) \gamma_5.
\end{aligned} \tag{19}$$

$B_i^+(p)$ accounts for chiral symmetry breaking in the normal propagator. $D_i^+(p)$ as well as $T_{B,i}^+(p)$ and $T_{D,i}^+(p)$ are only non-zero for color-superconducting phases with finite strange-quark masses. The self-energies are decomposed analogously.

The renormalization-point dependent light-quark condensate in the chiral limit is defined by

$$\langle \bar{u}u \rangle = \langle \bar{d}d \rangle = -Z_m Z_2 \sum_q \text{Tr}_{D,c}(S_{up}^+(q)). \tag{20}$$

where the Dirac and color trace of the up quark component of the quark propagator is performed.

Diquark condensates can be calculated analogously as

$$\mathcal{C}_i \equiv \langle \psi^T C \gamma_5 \mathcal{O}_i \psi \rangle = -Z_2 \sum_q \text{Tr}(\gamma_5 \mathcal{O}_i T^-(q)) \tag{21}$$

where \mathcal{O}_i is an operator in color-flavor space. In particular, we define \mathcal{C}_{ud} with

$$\mathcal{O}_{ud} = \frac{\tau_2}{2} \otimes \frac{\lambda_2}{2} = \frac{1}{4}(M_1 - M_2), \tag{22}$$

describing the mutual pairing of (red and green) non-strange quarks in the 2SC phase as well as in the CFL phase, and \mathcal{C}_{uds} with

$$\begin{aligned}
\mathcal{O}_{uds} &= \frac{1}{2} \left(\frac{\tau_5}{2} \otimes \frac{\lambda_5}{2} + \frac{\tau_7}{2} \otimes \frac{\lambda_7}{2} \right) \\
&= \frac{1}{8}(M_6 + M_7 - M_4 - M_5),
\end{aligned} \tag{23}$$

describing the pairing of non-strange quarks with strange quarks in the CFL phase.

These condensates represent the dominant pairing patterns in the color-superconducting phases under consideration. In a phase with exact CFL symmetry, \mathcal{C}_{ud} and \mathcal{C}_{uds} are equal, while in a CFL-like phase with heavier strange quarks, they can be different. In the 2SC phase, finally, \mathcal{C}_{uds} vanishes.

IV. TRUNCATION SCHEME

The quark DSE (1) and all other equations discussed so far are exact QCD equations. However, in order to solve

them, we need to specify the dressed gluon propagator and the dressed quark-gluon vertex, which enter the self-energy, eq. (2). In principle, they are given by their own DSEs but, since these involve even higher n-point functions, an exact solution would result in an infinite tower of equations. Therefore we have to rely on truncations. In this section we specify the truncation scheme used in the present work.

A. Dressed quark-gluon vertex

We begin with the dressed quark-gluon vertex, eq. (16). We restrict it to the diagonal NG components and an abelian ansatz

$$\Gamma_\mu^a(p, q) = \frac{\Lambda_a}{2} \gamma_\mu \Gamma(k), \tag{24}$$

with Λ_a as defined in eq. (15) and a dressing function Γ , which only depends on the gluon momentum $k = p - q$. For this function, we take a model ansatz, similar to the vertex proposed in Ref. [24]:

$$\frac{\Gamma(k)}{Z_2 \tilde{Z}_3} = \frac{d_1}{d_2 + k^2} + \frac{k^2}{k^2 + \Lambda^2} \left(\frac{\beta_0 \alpha(\nu) \ln(k^2/\Lambda^2 + 1)}{4\pi} \right)^{2\delta}. \tag{25}$$

Here \tilde{Z}_3 is the ghost propagator renormalization constant. The second term in parentheses describes the perturbative running in the ultraviolet, with $\beta_0 = (11N_c - 2N_f)/3$, $\delta = -9N_c/(44N_c - 8N_f)$ and a scale factor Λ . $\alpha(\nu) = g^2/4\pi$ is the strong fine-structure constant at the renormalization scale ν . Following Ref. [24], we take $\alpha(\nu) = 0.3$ and $\Lambda = 1.4$ GeV.

For the first term, which is relevant for the infrared behavior, we take $d_2 = 0.5$ GeV² [24] and fit d_1 to obtain a critical temperature of around 150 MeV for the chiral phase transition at $\mu = 0$. We get a value of $d_1 = 9.6$ GeV². As we will show in sect. VI this parametrization yields too large values for the chiral condensate and the pion decay constant in vacuum, whereas a fit to these quantities would yield a too low critical temperature. Since the focus of this article lies on the phase diagram, we consider a realistic critical temperature to be more important. We therefore continue with the parameters specified above. However, we will come back to this issue in sect. VI, where we introduce an alternative parametrization, fitted to vacuum quantities.

The vertex in Ref. [24] has additional contributions motivated by a Slavnov-Taylor identity and a Ball-Chiu vertex construction [34]. As there is no strict argument for the necessity of these components, we dropped them as they lead to instabilities in the iteration of color-superconducting phases.

In Landau gauge, the renormalization constant Z_{1F} , which appears in the bare vertex eq. (15), can be expressed as $Z_{1F} = Z_2/\tilde{Z}_3$ using Slavnov-Taylor identities. The normal and anomalous components of the self-energy

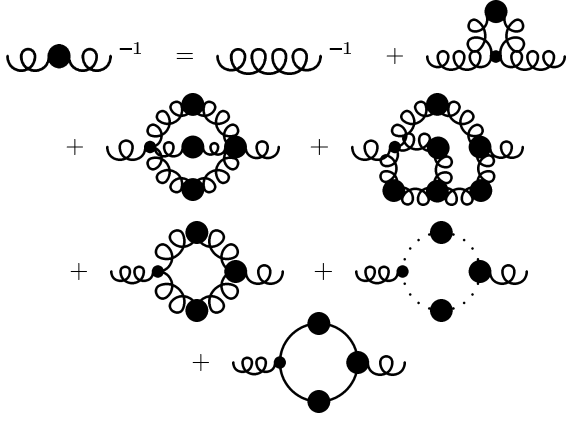


FIG. 2. DSE for the gluon propagator. Curly, dotted and plain lines represent gluon, ghost, and quark propagators, respectively. Thick dots indicate dressed quantities.

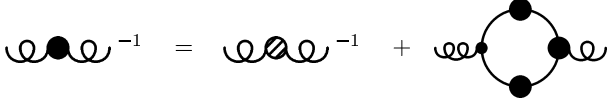


FIG. 3. Unquenching of the gluon propagator. The shaded propagator is the full Yang-Mills gluon propagator.

eq. (2) then become

$$\begin{aligned}\Sigma^+(p) &= 4\pi\alpha(\nu) \sum_q \frac{\Gamma(k)}{\tilde{Z}_3} \gamma_\mu \frac{\lambda_a}{2} S^+(q) \gamma_\nu \frac{\lambda_b}{2} D_{\mu\nu}^{ab}(k), \\ \Phi^+(p) &= -4\pi\alpha(\nu) \sum_q \frac{\Gamma(k)}{\tilde{Z}_3} \gamma_\mu \frac{\lambda_a^T}{2} T^+(q) \gamma_\nu \frac{\lambda_b}{2} D_{\mu\nu}^{ab}(k),\end{aligned}\quad (26)$$

where k is again the gluon momentum $p - q$. Note that \tilde{Z}_3 drops out when eq. (25) is inserted.

B. Dressed gluon propagator

The gluon DSE is depicted in fig. 2. Restricting this equation to the first three lines corresponds to the pure (“quenched”) Yang-Mills system, while the last diagram describes the coupling to the quarks. Solving the Yang-Mills equations is numerically demanding already without quarks [35–37]. In recent years significant progress has been made in this sector by combining continuum methods with lattice calculations. Therefore we consider a truncated version of the full gluon DSE, where we take the solution of the quenched Yang-Mills equations as input and include the quark effects only perturbatively. This scheme is depicted in fig. 3. It neglects back-coupling effects of the quark propagator on the Yang-Mills sector but should carry the dominant effects of the quark loop on the gluon propagator.

The gluon DSE is then given by

$$D_{\mu\nu}^{-1,ab}(k) = D_{\mu\nu,YM}^{-1,ab}(k) + \Pi_{\mu\nu}^{ab}(k) \quad (27)$$

with the Yang-Mills gluon propagator $D_{\mu\nu,YM}^{ab}$ and the gluon polarization tensor $\Pi_{\mu\nu}^{ab}$. The former has the same transverse Dirac structure as the full gluon propagator, eq. (3), and is diagonal in color space,

$$D_{\mu\nu,YM}^{ab}(k) = \left(\frac{Z_{TT}^{YM}(k)}{k^2} P_{\mu\nu}^T(k) + \frac{Z_{TL}^{YM}(k)}{k^2} P_{\mu\nu}^L(k) \right) \delta^{ab}. \quad (28)$$

For the dressing functions we adopt the parametrizations of Ref. [25],

$$\begin{aligned}Z_{TT,TL}^{YM}(k) &= \frac{k^2 \Lambda^2}{(k^2 + \Lambda^2)^2} \left(\left(\frac{c}{k^2 + a_{T,L} \Lambda^2} \right)^{b_{T,L}} \right. \\ &\quad \left. + \frac{k^2}{\Lambda^2} \left(\frac{\beta_0 \alpha(\nu) \ln(k^2/\Lambda^2 + 1)}{4\pi} \right)^\gamma \right),\end{aligned}\quad (29)$$

which have been obtained by fitting lattice results. The scale factor Λ and the parameters describing the perturbative behavior in the UV are the same as in eq. (25). The exponent $\gamma = (-13N_c + 4N_f)/(22N_c - 4N_f)$ is related to δ by $2\delta + \gamma = -1$. The infrared behavior is parametrized by a temperature-independent constant $c = 11.5 \text{ GeV}^2$ and temperature-dependent parameters $a_{T,L}$ and $b_{T,L}$, which are tabulated in Ref. [25] for various temperatures. We determine their values at other temperatures by linear interpolation.

The polarization tensor is given by

$$\Pi_{\mu\nu}^{ab}(k) = -\frac{g^2}{2} \sum_q \text{Tr} (\Gamma_\mu^{a,0} \mathcal{S}(p) \Gamma_\nu^b(p, q) \mathcal{S}(q)) \quad (30)$$

with $p = k + q$. It depends, in principle, on the dressed quark propagator, but, as a further simplification, we will evaluate it with bare quark propagators in HTL-HDL approximation (see sect. IV C). The trace has to be carried out in Dirac, color, flavor and Nambu-Gorkov space. As quantum corrections must not change the transverse nature of the gluon, see Eqs. (3) and (28), we require the polarization tensor to be transverse as well, *i.e.*,

$$\Pi_{\mu\nu}^{ab}(k) = \Pi_{TT}^{ab}(k) P_{\mu\nu}^T(k) + \Pi_{TL}^{ab}(k) P_{\mu\nu}^L(k). \quad (31)$$

The dressed gluon propagator is then given by

$$\begin{aligned}D_{\mu\nu}^{ab}(k) &= \frac{Z_{TT}^{YM}(k)}{k^2 + Z_{TT}^{YM}(k) \Pi_{TT}^{ab}(k)} P_{\mu\nu}^T(k) \\ &\quad + \frac{Z_{TL}^{YM}(k)}{k^2 + Z_{TL}^{YM}(k) \Pi_{TL}^{ab}(k)} P_{\mu\nu}^L(k).\end{aligned}\quad (32)$$

C. HTL-HDL approximation

Since the gluon polarization tensor eq. (30) depends on the dressed quark propagator, eq. (32) must, in principle,

be solved self-consistently together with the quark DSE. However, in a first step, we perform a simpler non-self-consistent approximation, which was also employed in Ref. [28, 29].

In this scheme, we neglect the vacuum part of the polarization loop and calculate the medium corrections in hard-thermal-loop-hard-dense-loop (HTL-HDL) approximation, using the bare propagator of massless quarks,

$$(S^+)^{-1}(p) = -i(\omega_n + i\mu)\gamma_4 - i\vec{p}. \quad (33)$$

In the HTL-HDL approximation, it is assumed that the external momenta are small compared to the chemical potential or temperature. This allows for an approximate analytical evaluation of the loop integral. The result can be found in textbooks, *e.g.*, Ref. [38], and is given by

$$\begin{aligned} Z_{TT}^{YM}(k)\Pi_T^{ab}(k) &= \\ m_{TT}^2 \frac{\omega_m}{|\vec{k}|} \left[\left(1 + \left(\frac{\omega_m^2}{\vec{k}^2} \right) \right) iQ \left(\frac{i\omega_m}{|\vec{k}|} \right) - \frac{\omega_m}{|\vec{k}|} \right] \delta^{ab} \\ Z_{TL}^{YM}(k)\Pi_L^{ab}(k) &= \\ 2m_{TL}^2 \frac{\omega_m^2 + \vec{k}^2}{\vec{k}^2} \left[1 - \frac{\omega_m}{|\vec{k}|} iQ \left(\frac{i\omega_m}{|\vec{k}|} \right) \right] \delta^{ab} \end{aligned} \quad (34)$$

with

$$iQ(ix) = \frac{i}{2} \ln \frac{ix+1}{ix-1} = \arctan\left(\frac{1}{x}\right). \quad (35)$$

and bosonic Matsubara frequencies $\omega_m = 2m\pi T$. The effective transverse and longitudinal gluon masses are defined by

$$m_{TT,TL}^2 = N_f \alpha_{TT,TL}(k) \left(\frac{\pi T^2}{3} + \frac{\mu^2}{\pi} \right) \quad (36)$$

with the renormalization-point independent running couplings, which are given by [28]

$$\alpha_{TT,TL}(k) = \frac{\Gamma(k)Z_{TT,TL}^{YM}(k)}{Z_2\tilde{Z}_3}\alpha(\nu). \quad (37)$$

In this approximation, all quark-mass effects and color-superconducting contributions to the polarization tensor are neglected, but, as it provides analytical results for the gluon polarization, it has the advantage to keep the numerical effort at the same level as in a pure rainbow truncation with quenched gluons.

An extended truncation scheme, where the solutions of the quark DSE are self-consistently used in the gluon polarization tensor, will be discussed in a forthcoming paper [39].

D. Strange-quark mass

The last input quantity to be specified is the strange-quark mass at the renormalization scale ν . According to the particle data group (PDG) [40], its value is

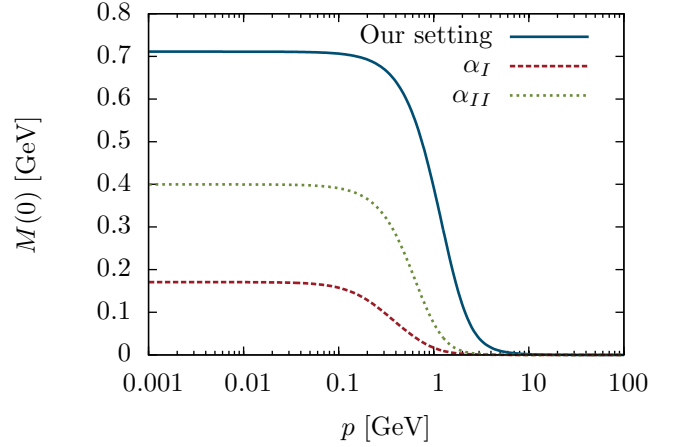


FIG. 4. Vacuum-mass functions $M(p) = B_1^+(p)/A_1^+(p)$ of chiral quarks ($m = 0$) for the interactions $\alpha_{I,II}$ from [29] and in our setting.

$m_s = 95 \pm 5$ MeV in the \overline{MS} renormalization scheme at a renormalization scale of $\nu = 2$ GeV. In earlier Dyson-Schwinger calculations [29] the renormalization point was therefore chosen to be $\nu = 2$ GeV as well, and the PDG value for m_s was directly used as an input.

However, as already pointed out in the Introduction, the gluon dressing functions and vertices used in Ref. [29] differ from ours, which has a strong effect on the mass functions. This is illustrated in fig. 4, where the vacuum-mass functions of the (chiral) up and down quarks are shown for the two interactions used in Ref. [29] and for the present setting.

An essential difference is that, for the former, the chiral symmetry restoration sets in at lower momenta. As a consequence, $p = 2$ GeV already belongs to the perturbative regime, so that the perturbative strange-quark mass could be used at this scale. In contrast, with the improved parametrizations of quark-gluon vertex and gluon propagator used in our calculations, there are still considerable non-perturbative effects at 2 GeV, and therefore we have to renormalize at a higher scale to be in the perturbative region. To be on the safe side, we choose $\nu = 100$ GeV.

The renormalization scheme used in this work is a momentum subtraction (MOM) scheme. We can therefore take the MOM-scheme value of the strange-quark mass obtained in the lattice calculation of Ref. [41] and evolve it to our renormalization point $\nu = 100$ GeV with a four-loop running [42]. Assuming an error band of the same order as in the PDG, we find a strange-quark mass $m_s(100 \text{ GeV}) = 55 - 62$ MeV.

On the other hand, the scale factor $\Lambda = 1.4$ GeV in Eqs. (25) and (29), which was taken from Ref. [24], is higher than the expected MOM scale, and it is not clear whether the perturbatively evolved strange-quark mass is consistent with our truncation. A larger scale leads to a stronger increase of the quark mass in the infrared. This could be important, as a large strange-quark mass

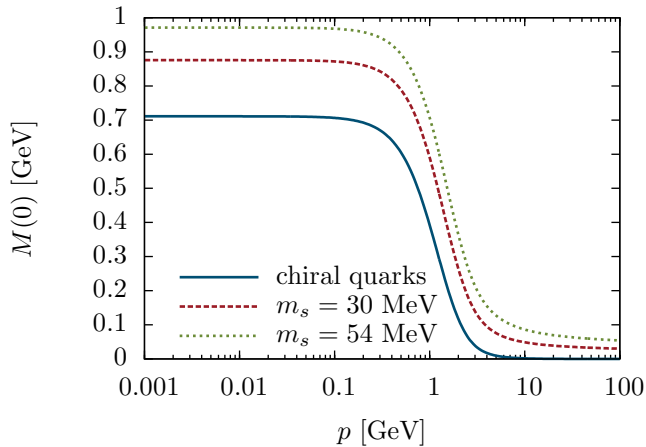


FIG. 5. Vacuum-mass functions $M(p)$ of chiral quarks ($m = 0$) and strange quarks ($m = 30$ MeV, $m = 54$ MeV).

disfavors the CFL phase relative to the 2SC phase. Since, as mentioned in the Introduction, the existence of the 2SC phase at intermediate chemical potentials will be our central result, we have to make sure that this is not an artifact of a too large choice for m_s . We therefore take the above result of the evolution as an upper limit and additionally consider a smaller strange-quark mass to check the stability of the 2SC phase. To be specific, we perform calculations with $m_s = 54$ MeV and with $m_s = 30$ MeV at $\nu = 100$ GeV.

The corresponding mass functions $M(p)$ in vacuum are shown in fig. 5, together with the mass function of the chiral ($m = 0$) up and down quarks. For the latter we find $M(0) = 710$ MeV, while for the strange quarks we obtain $M(0) = 875$ MeV for $m_s = 30$ MeV and $M(0) = 970$ MeV for $m_s = 54$ MeV. These values seem to be unrealistically large, when we compare them with typical constituent quark masses in phenomenological models. Indeed, as mentioned earlier, our fit of the vertex parameters to the chiral critical temperature at $\mu = 0$ tends to overestimate the strength of chiral symmetry breaking in vacuum (see sect. VI). In an improved truncation scheme, which will be discussed in a future publication [39], we obtain smaller masses at $p = 0$, which are of the order of 450 MeV for up and down quarks and 600 to 700 MeV for strange quarks. It should be emphasized, however, that the quark masses are not observable. Moreover, the size of the non-perturbative regime will roughly stay the same.

V. RESULTS

The temperature dependence of the (non-strange) chiral condensate at $\mu = 0$ is shown in fig. 6. The condensate decreases with increasing temperature until chiral symmetry is restored in a second-order phase transition at around $T = 150$ MeV. The small kinks are due to the temperature-dependent lattice input.

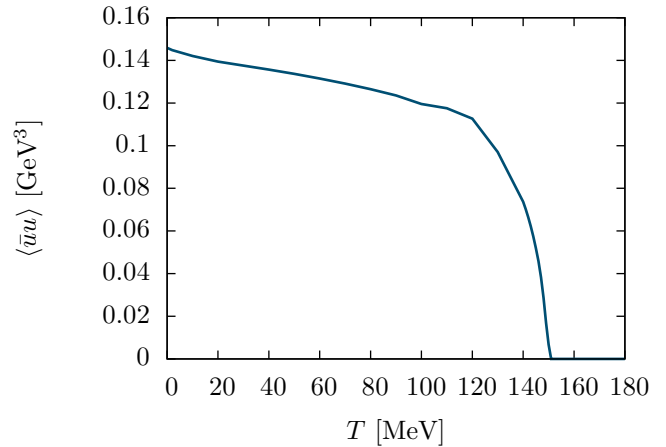


FIG. 6. Temperature-dependence of the chiral condensate $\langle \bar{u}u \rangle$ at the renormalization scale $\nu = 100$ GeV at $\mu = 0$.

In fig. 7 we show the diquark condensates defined in eqs. (21) – (23) at low temperatures, $T = 10$ MeV, as functions of the chemical potential. As discussed in sect. III, our formalism allows for the description of both 2SC and CFL-like pairing. Since the condensate C_{ud} , related to the mutual pairing of up and down quarks, is present in both phases, we indicate explicitly in which phase the solutions have been obtained. We also do so for the condensate C_{uds} , although it is non-zero only in the CFL phase. In addition, there is always a non-superconducting solution, where all diquark condensates vanish. This is not shown in the figure.

The upper and the lower panel of fig. 7 correspond to $m_s = 30$ MeV and 54 MeV, respectively. The qualitative behavior is similar in both cases, and even the quantitative differences are not large. All condensates rise with increasing chemical potential. At lower values of μ , we only find a 2SC solution of the DSE, whereas above a threshold of about 500 or 600 MeV, depending on m_s , there is also a CFL-like solution.

This behavior is related to the μ -dependence of the dynamical quark masses, which are displayed in fig. 8. Since the normal and color-superconducting dressing functions are mutually coupled through the DSEs, the dynamical quark masses depend on the phase as well. At low μ we find a non-superconducting solution with spontaneously broken chiral symmetry, where the up and down quarks have relatively large masses (dash-dotted) line. On the other hand, there is always a 2SC solution with massless up and down quarks. In the CFL-like solutions, the up and down quarks are almost massless as well¹. The

¹ In the CFL phase, the up and down quarks have a small mass (< 2 MeV), which is induced by their coupling to the massive strange quarks. This is possible because the CFL condensates break the chiral $SU(2)$ symmetry. The situation is further complicated by the fact that red up, green down, and blue strange quarks are mixed in the CFL phase (see eq. (A1)). In princi-

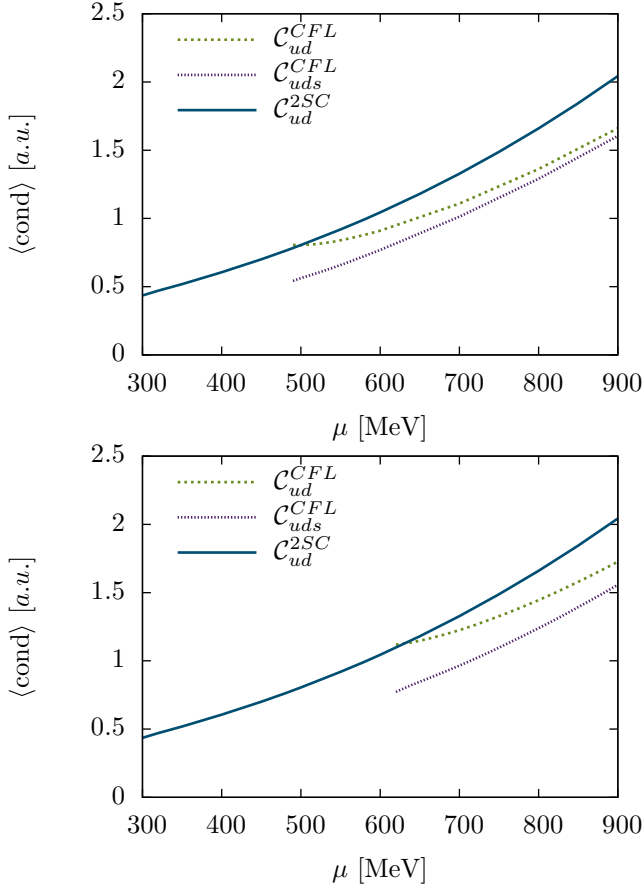


FIG. 7. Dependence of 2SC and CFL condensates at $T = 10$ MeV on the chemical potential for $m_s = 30$ MeV (top) and $m_s = 54$ MeV (bottom). All condensates are given in arbitrary, but equal, units.

strange quarks, on the other hand, are quite heavy at low and intermediate chemical potentials. As a consequence, the Fermi momenta of strange and non-strange quarks are very different, so that their mutual pairing is inhibited. However, with increasing chemical potential, the strange quarks become lighter and eventually undergo a crossover to even smaller masses. This effect, which is seen in the 2SC phase (dashed line), also triggers the onset of CFL-like solutions. In the latter the strange-quark mass (dotted line) is slightly lower than in the former, but the difference is small and almost vanishes at very high μ , where the mass is dominated by perturbative effects.

As discussed earlier, the quark masses are neglected in the gluon polarization function in the HTL-HDL truncation. Therefore, if there is no pairing between strange and non-strange quarks, the strange sector decouples from the non-strange sector. As a consequence, the strange-quark mass is not affected by a possible chiral phase transition

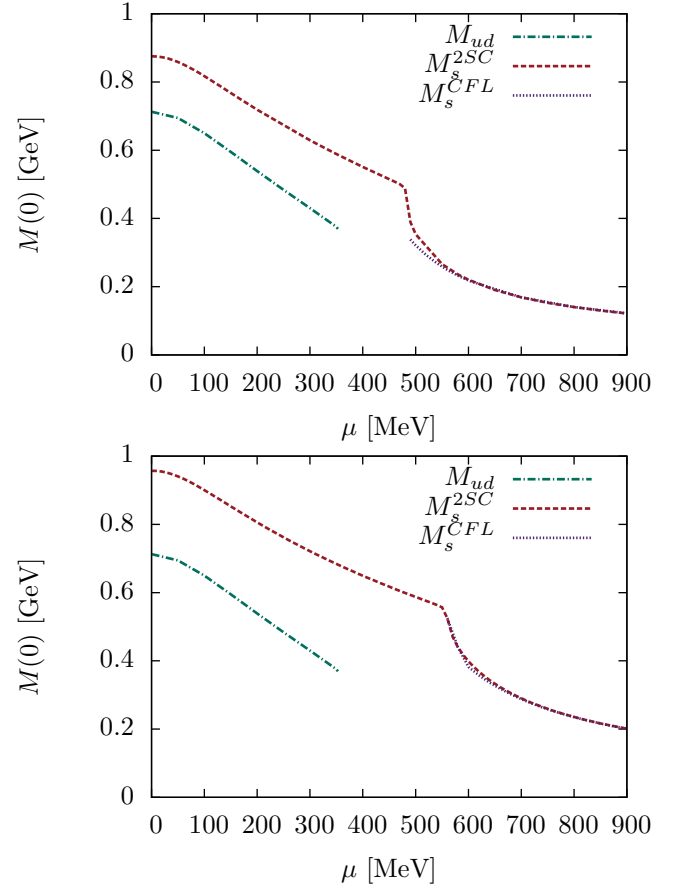


FIG. 8. Dynamical quark masses $M(0) = B^+(0)/C^+(0)$ as functions of the chemical potential at $T = 10$ MeV for $m_s = 30$ MeV (top) and $m_s = 54$ MeV (bottom). The up- and down-quark masses are only shown for the non-superconducting chirally broken phase. They vanish in the 2SC phase and are very small in the CFL phase.

of the up and down quarks. Likewise, \mathcal{C}_{ud}^{2SC} does not depend on m_s and is not influenced by the rapid change of M_s in the crossover region.

In fig. 9 the temperature dependence of the diquark condensates is shown for $m_s = 30$ MeV at a chemical potential of $\mu = 580$ MeV and for $m_s = 54$ MeV at $\mu = 680$ MeV (lower panel). The 2SC condensate smoothly decreases with increasing temperature and eventually vanishes at a temperature between 20 and 25 MeV. In contrast, the CFL-like solution ceases to exist already above a lower critical temperature, where the condensates are still finite. This behavior suggests that, with increasing T , the system first undergoes a first-order phase transition from the CFL phase to the 2SC phase, followed by a second-order phase transition to the normal-conducting phase.

However, if there are several solutions of the DSE at given temperature and chemical potential, the favored phase can only be determined by comparing the corresponding pressures. The pressure is equal to the effective

ple, one should therefore project on the different quasi-particle modes. However, for simplicity, we just show the P_6 component in fig. 8, corresponding to red and green strange quarks.

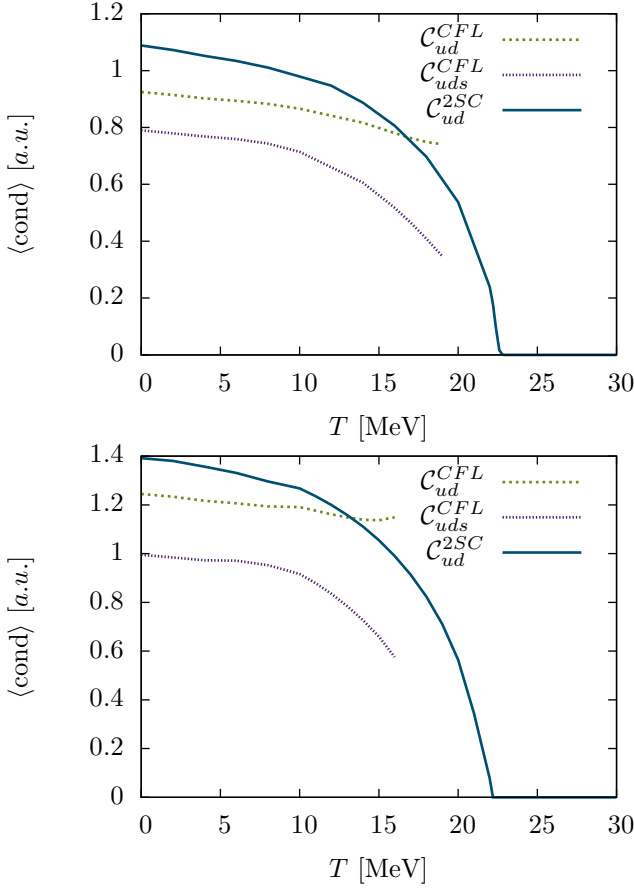


FIG. 9. Temperature dependence of 2SC and CFL condensates at $\mu = 580$ MeV for $m_s = 30$ MeV (top) and at $\mu = 680$ MeV for $m_s = 54$ MeV (bottom). The units are the same as in Fig. 7.

action, which in general is given by

$$\Gamma = \oint_p \frac{1}{2} \text{Tr} \ln \mathcal{S}^{-1}(p) - \oint_p \frac{1}{2} \text{Tr} (1 - Z_2 \mathcal{S}_0^{-1}(p) \mathcal{S}(p)) + \Gamma_2. \quad (38)$$

Here Γ_2 denotes the two-particle irreducible part. Our present truncation with HTL-HDL approximation corresponds to the expression

$$\Gamma_2 = g^2 \oint_p \oint_q \frac{1}{4} \text{Tr} (\Gamma_{\mu,0}^a \mathcal{S}(p) D_{\mu\nu}^{ab}(p-q) \Gamma_\nu^b(p,q) \mathcal{S}(q)). \quad (39)$$

The resulting pressure is quartically divergent. Although finite expressions can be obtained by calculating pressure differences between competing phases [29], unfortunately the results are numerically very unstable. This is due to the fact that the convergence behavior is determined by the high-energy tails of the integrands, which contain only little information about the phase under consideration.

We therefore proceed as follows. As argued in appendix B, there are reasons to believe that the solu-

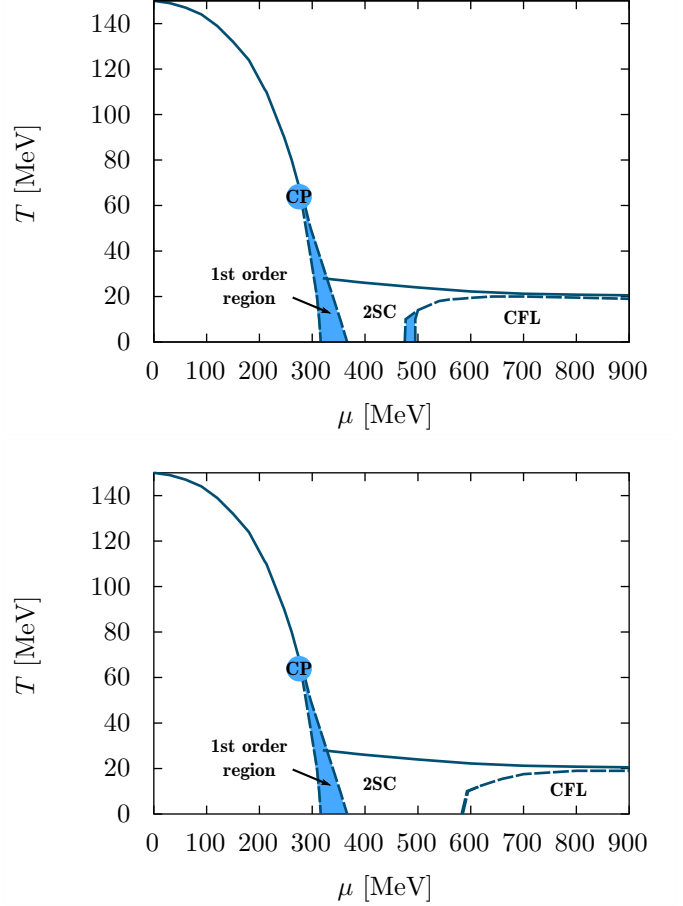


FIG. 10. Phase diagram for $m_s = 30$ MeV (top) and $m_s = 54$ MeV (bottom). The shaded areas indicate the region of the first-order phase transition, bounded by spinodal lines (dashed). Solid lines indicate second-order phase transitions, CP denotes the tricritical point.

tions found by solving the DSEs iteratively, correspond to global or local maxima of the pressure, *i.e.*, to stable or metastable solutions, but not to unstable ones. According to this hypothesis (which is often assumed in DSE calculations), this means that we always find the correct solution in the case of second-order phase transitions.

For first-order phase transitions, the situation is more complicated. In this case, there is a certain regime, where a stable and a metastable solution of the DSE exist, which both can be found by iteration. The exact position of the phase transition, which manifests itself in a jump between the two solutions, can then only be determined by studying the pressure of the system. However, because of the numerical uncertainties mentioned above, in practice this does not further narrow down the phase-transition region. We therefore restrict ourselves to calculating the spinodal lines of the first-order region, *i.e.*, the lines where the metastable solutions disappear. As these regions mostly have only a small extent, they still give a good estimate for the phase boundary.

The resulting phase diagrams are shown in fig. 10. Again, the upper and lower panels correspond to $m_s = 30$ MeV and 54 MeV, respectively. As pointed out earlier, in the HTL-HDL approximation, the strange and non-strange sectors decouple, except for the CFL phase, where they are coupled by the condensate. Therefore the only effect of m_s on the phase diagram is a shift of the CFL phase boundary.

The shaded areas indicate first-order regions bounded by spinodal lines. The most prominent ones correspond to the chiral phase transition from the chirally broken phase to the 2SC phase or, at somewhat higher temperatures, to the non-superconducting chirally restored phase (with respect to the up and down quarks). The spinodal region and, hence, the first-order phase transition inside this region end at a tricritical point at $T = 60$ MeV and $\mu = 300$ MeV. Above this point, the chiral phase transition is of second order.

The temperature of the tricritical point is lower than in the DSE analysis of Ref. [26], where it was found at $T = 95$ MeV and $\mu = 280$ MeV. The authors use a similar truncation scheme but consider only two flavors. This also leads to a higher critical temperature of 180 MeV at $\mu = 0$. As shown in Ref. [27], the inclusion of strange quarks reduces the temperature of the critical point and shifts it to a slightly higher chemical potential. This is consistent with our result. However, since in Ref. [27] a truncation without the HTL-HDL approximation was used, a direct comparison of the 2 + 1-flavor results with ours is not possible.

The low- μ part of the phase diagram and the region around the critical point are mainly shown for completeness, while our focus is on the color-superconducting phases at low temperatures and higher chemical potentials. Here we find a 2SC phase, followed by a CFL phase. The latter is favored above ~ 500 MeV for $m_s = 30$ MeV and ~ 600 MeV for $m_s = 54$ MeV. The 2SC phase also extends to somewhat higher temperature than the CFL phase (cf. Fig. 9) and, thus, separates the latter from the normal-conducting chirally restored phase. The phase transition between 2SC and restored phase is second order and takes place around 20 – 30 MeV. Remarkably, the critical temperature is slowly decreasing with increasing chemical potential, despite the fact that the zero-temperature condensate increases (cf. Fig. 7).

As is clear from the discussion of Fig. 7, the phase transition between 2SC and CFL phase at low temperature is first order. However, the spinodal region turns out to be very narrow and only visible for low temperatures at $m_s = 30$ MeV². Moreover, we have numerical indications

that at large μ the phase transition is second order, *i.e.*, the spinodal region ends again in a critical point. Such a behavior was also found in the NJL-model analysis of Ref. [20]. For $m_s = 30$ MeV, the critical point seems to be somewhere around $\mu = 900$ MeV, but it is difficult to localize its position exactly.

VI. ALTERNATIVE PARAMETRIZATION

As pointed out before, the parametrization of the quark-gluon vertex function used so far, yields too large values for the pion decay constant and the chiral condensate in vacuum. In this section, we will discuss this in more detail. It raises the question to what extent the results presented in the previous section, and in particular the existence of a 2SC phase at intermediate chemical potentials, are consequences of a potentially too strong attraction in the infrared. We will therefore determine an alternative parametrization by fitting vacuum observables instead of the chiral critical temperature. Afterwards, we present the resulting phase diagram.

A. Chiral condensate and pion decay constant

For massless quarks the renormalization dependent chiral condensate can be calculated with eq. (20). For the parametrization used so far this yields the vacuum value $\langle \bar{u}u \rangle(\nu) = -0.14 \text{ GeV}^3$ at our renormalization point $\nu = 100 \text{ GeV}$ (cf. fig. 6). However, for comparison with literature values, we need the renormalization-point independent condensate. Employing the operator product expansion, this quantity can be extracted by fitting the asymptotic behavior of the quark-mass function [43]

$$M(p) \stackrel{p \rightarrow \infty}{\sim} -\langle \bar{u}u \rangle \frac{2\pi^2 \gamma_m}{3p^2} \left(\frac{1}{2} \log(p^2/\bar{\Lambda}^2) \right)^{\gamma_m - 1} \quad (40)$$

with the anomalous dimension $\gamma_m = 12/(11N_c - 2N_f)$. In a full calculation, the parameter $\bar{\Lambda}$ would correspond to Λ_{QCD} . As we solve a truncated system, its value can be different and we treat it as a fit parameter as well. We then get a value of $\langle \bar{u}u \rangle = -(425 \text{ MeV})^3$ for the renormalization-point independent condensate.

The pion decay constant can be estimated with the Pagels-Stokar formula [44, 45]

$$f_\pi^2 = \frac{N_c}{4\pi^2} \int_0^\infty dp^2 p^2 \frac{Z_2 A^{-1}(p^2) M(p^2)}{(p^2 + M^2(p^2))^2} \left(M(p^2) - \frac{p^2}{2} \frac{dM(p^2)}{dp^2} \right). \quad (41)$$

For the parametrization used so far, we get $f_\pi = 127 \text{ MeV}$.

² This means that the 2SC solution is unstable almost everywhere where a CFL solution exists. The 2SC condensates shown in Figs. 7 and 9 have been obtained by forcing the strange condensates to be exactly zero during the iteration. Otherwise, starting with a small non-vanishing strange condensate, the iteration only converges to the 2SC solution if we are outside the CFL regime or in the very small spinodal region.

B. Vacuum fit

Hence, both, the chiral condensate and the pion decay constant, are too large compared with realistic values $\langle \bar{u}u \rangle \approx -(250 \text{ MeV})^3$ and $f_\pi = 92.4 \text{ MeV}$ (or $f_\pi = 88 \text{ MeV}$ in the chiral limit). This deviation suggests that the infrared enhancement of the quark-gluon vertex, which is mainly determined by the parameters d_1 and d_2 in eq. (25), is possibly too strong. Indeed, we can easily obtain a better fit of f_π by choosing a smaller value of d_1 . It turns out, however, that in order to get sufficiently strong reduction of the chiral condensate, we also have to modify the scale of the logarithmic running and the parametrization of the gluon dressing functions.

In fact, the lattice calculation of the gluon propagator only provides data up to a few GeV, leaving some freedom for the parameters in eq. (29). In the new parametrization, we take $a_T = a_L = 1.01$, $b_T = b_L = 0.8$, $c = 16.3 \text{ GeV}^2$, $\alpha(\nu) = 0.727$ and $\Lambda = 1.160 \text{ GeV}$. For the logarithmic running in the expression $\ln(k^2/\bar{\Lambda}^2 + 1)$ we choose a smaller scale of $\bar{\Lambda} = 0.6 \text{ GeV}$. There is no need to introduce temperature dependent parameters, since we will stay below $T \approx 100 \text{ MeV}$, where the lattice data are almost temperature independent.

For the vertex dressing we use the parametrization

$$\Gamma(k) = Z_2 \tilde{Z}_3 \frac{\Lambda^2}{k^2 + \Lambda^2} \left(\left(\frac{d_1}{d_2 + k^2} \right)^2 + \frac{k^2}{\Lambda^2} \left(\frac{\beta_0 \alpha(\nu) \ln(k^2/\bar{\Lambda}^2 + 1)}{4\pi} \right)^{2\delta} \right) \quad (42)$$

with $d_1 = 3.15 \text{ GeV}^2$, $d_2 = 0.5 \text{ GeV}^2$, and Λ and $\bar{\Lambda}$ as specified above.

With this choice we obtain the realistic vacuum values $f_\pi = 87.5 \text{ MeV}$ and $\langle \bar{u}u \rangle = -(260 \text{ MeV})^3$. The latter corresponds to a renormalization-point dependent condensate of -0.035 GeV^3 at $\nu = 100 \text{ MeV}$. We can then employ the Gell-Mann–Oakes–Renner relation, $f_\pi^2 m_\pi^2 = -2m_{u,d} \langle \bar{u}u \rangle$ to estimate the value of the up and down quarks at this scale. Taking $m_\pi = 135 \text{ MeV}$, this yields $m_{u,d} = 2 \text{ MeV}$. Finally, since the mass ratio of strange and non-strange quark is $m_s/m_{u,d} = 27.5$ [40], we conclude that the strange-quark mass is about 55 MeV . In the following, we will therefore restrict ourselves to our larger value of the strange-quark mass, $m_s(\nu = 100 \text{ GeV}) = 54 \text{ MeV}$, and take chiral up and down quarks, as before.

C. Phase diagram

The phase diagram obtained with this parametrization is shown in fig. 11. To first approximation, it looks similar to the phase diagrams in fig. 10 but with all critical temperatures and chemical potentials reduced by about 30%. In particular the chiral phase transition temperature at $\mu = 0$ is way below the lattice value of about

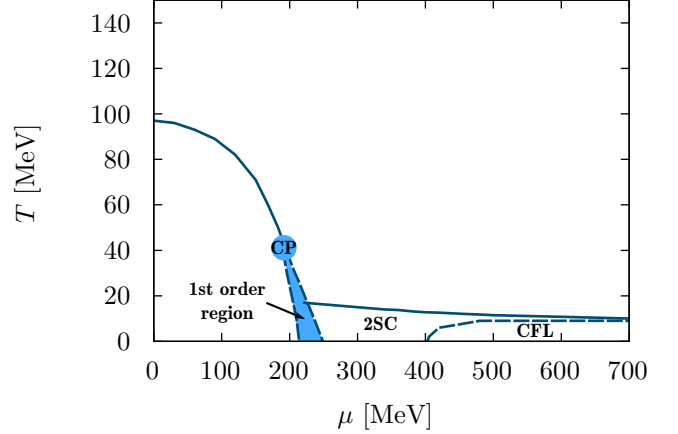


FIG. 11. Phase diagram for a parametrization fixed by vacuum quantities.

150 MeV. Also the critical chemical potential at $T = 0$ is totally unrealistic, as it is below the nuclear-matter point, $\mu_{nm} = 308 \text{ MeV}$. We will come back to this problem in the Conclusions below.

Our main result at this point is that the qualitative phase structure is very similar as for our previous parametrization. In particular, we still find a region with a stable 2SC phase.

VII. CONCLUSIONS AND OUTLOOK

We have investigated color-superconducting phases in QCD with Dyson-Schwinger equations in Landau gauge. For the gluon propagator we used a recent parametrization of quenched lattice data and included quark-loop effects perturbatively in a hard-thermal-loop-hard-dense-loop approximation. For the vertex we used a phenomenological ansatz constrained by the known asymptotic behavior in the ultraviolet, while the infrared strength is fitted to obtain a chiral phase-transition temperature of 150 MeV at $\mu = 0$.

We have studied 2SC and CFL-like phases for $N_f = 2+1$ flavors with chiral up and down quarks, and massive strange quarks. We find a dominant CFL phase at high chemical potentials and low temperatures while there is always a thin 2SC band at higher temperature, separating the CFL phase from the non-superconducting chirally restored phase. The transition to the latter takes place at critical temperatures around $T = 20 - 30 \text{ MeV}$.

Our most important result is that we also find a stable 2SC phase at small temperatures and intermediate chemical potential, $\mu \lesssim 500 \text{ MeV}$. This is in strong contrast to the results of Ref. [29] where the CFL phase was found to be favored practically all the way down to the hadronic phase at zero temperature.

The difference should therefore mainly be attributed to the improved gluon propagators and vertices, which we

have used. This interaction is effectively stronger than those used in Ref. [29]. As a consequence, the strange quarks stay heavy up to higher chemical potentials, inhibiting their pairing with the non-strange quarks.

On the other hand, the vacuum values for the chiral condensate and the pion decay constant obtained with this parametrization are much too large. We have therefore performed calculations with an alternative parametrization, where these vacuum quantities have been fitted to their empirical values. We found that the resulting phase structure stays qualitatively unchanged and the stable 2SC region persists. The critical temperatures and chemical potentials are, however, too small.

This observation that we were not able to obtain a good vacuum fit and a reasonable critical temperature simultaneously is clearly the most unsatisfactory feature of the employed truncation scheme. In fact, the HTL-HDL approximation neglects quark-mass and pairing-gap effects on the quark-polarization loop in the gluon propagator and therefore overestimates the gluon screening in the chirally broken and color superconducting phases. Therefore we are currently working on an improved scheme, where the dressed Nambu-Gorkov propagators from the quark DSE are self-consistently used to evaluate the polarization loop. Preliminary results indicate that this leads to quantitative changes, bridging the gap between the parametrizations fitted to vacuum quantities or to the chiral phase transition, respectively. In particular, when the parameters are fitted to the chiral critical temperature $T = 150$ MeV, the dressed quark masses and the pion decay constant are considerably lower than in HTL-HDL approximation. Also, the critical temperatures for CSC phases increase. However, the structure of the phase diagram is not altered qualitatively and the stable 2SC phase persists [39].

Further possible improvements concern the quark-gluon vertex, which is only constrained in the UV so far, while for the IR behavior we used a phenomenological model ansatz. It has been studied on the lattice [46] and also with Dyson-Schwinger equations in semi-perturbative truncations [47, 48]. Recently the coupled system of quark DSE and vertex DSE has been investigated self-consistently in a truncated version in vacuum [49] and it is desirable to include non-abelian vertex structures and finally to implement a truncated vertex DSE self-consistently. However, studies of the vertex DSE in medium are very difficult and have not been performed so far.

In the present paper, we have considered a single, flavor independent chemical potential. These studies should be extended to electrically neutral matter in beta equilibrium, as relevant for compact stars. Such an analysis has been performed in Ref. [30] for zero temperature using the “old” gluonic interaction. Since electric neutrality splits the Fermi surfaces of up and down quarks, it disfavors the 2SC phase [50]. Therefore, it would be interesting to see, whether this phase survives when the improved interaction is used.

Another interesting question is, whether the QCD phase diagram contains inhomogeneous phases. Phases with spatially varying chiral condensates have been found in effective models [51, 52] and in large- N_c QCD with weak-coupling methods [53, 54]. It would be exciting to study these phases with DSEs as well. This also includes inhomogeneous color superconductors [55–57], which may exist when electric neutrality is enforced.

Finally, it is an important, but difficult, task to calculate the pressure in the various phases, which would allow for a more precise determination of the first-order phase boundaries. Although an analytical expression for the pressure is given by the effective potential, its numerical evaluation was so far hindered by the poor convergence of the integrals. A solution of this problem would constitute a major breakthrough.

VIII. ACKNOWLEDGEMENTS

We would like to thank Christian Fischer and Jan Lücker for helpful discussions and comments. D.M. was supported by BMBF under contract 06DA9047I and by the Helmholtz Graduate School for Hadron and Ion Research. M.B. and J.W. acknowledge partial support by the Helmholtz International Center for FAIR and by the Helmholtz Institute EMMI.

Appendix A: Color-flavor structure

The matrices P_i and M_i , which parametrize the color-flavor structure of the quark propagator and self-energies, Eqs. (17) and (18), are constructed such that they yield a closed set of self-consistency equations when inserted into eq. (10). Additional restrictions come from the requirement that the resulting propagator must be consistent with the symmetries of the considered phase.

In the most general case considered here, the CFL-like pairing pattern with finite strange-quark mass, the residual color-flavor symmetry is $SU_{c+V}(2) \otimes U_{c+V}(1)$, generated by $\tau_a - \lambda_a^T$ with $a = 1, 2, 3$, and 8. One then finds that the sets $\{P_i\}$ and $\{M_i\}$ consist of seven matrices each [29]. In the color-flavor basis $\{(r, u), (g, d), (b, s), (r, d), (g, u), (r, s), (b, u), (g, s), (b, d)\}$ these are given by

$$P_i = \begin{pmatrix} \delta_{i,1} + \delta_{i,2} & \delta_{i,2} & \delta_{i,4} & & & & & & & \\ & \delta_{i,2} & \delta_{i,1} + \delta_{i,2} & \delta_{i,4} & & & & & & \\ & \delta_{i,5} & \delta_{i,5} & \delta_{i,3} & & & & & & \\ & & & & \delta_{i,1} & & & & & \\ & & & & & \delta_{i,1} & & & & \\ & & & & & & \delta_{i,6} & & & \\ & & & & & & & \delta_{i,7} & & \\ & & & & & & & & \delta_{i,6} & \\ & & & & & & & & & \delta_{i,7} \end{pmatrix}, \quad (\text{A1})$$

$$M_i = \begin{pmatrix} \delta_{i,1} + \delta_{i,2} & \delta_{i,2} & \delta_{i,4} & & & & \\ \delta_{i,2} & \delta_{i,1} + \delta_{i,2} & \delta_{i,4} & & & & \\ \delta_{i,5} & \delta_{i,5} & \delta_{i,3} & & & & \\ & & & \delta_{i,1} & & & \\ & & & \delta_{i,1} & & & \\ & & & & \delta_{i,7} & & \\ & & & & \delta_{i,6} & & \\ & & & & & \delta_{i,7} & \\ & & & & & & \delta_{i,6} \end{pmatrix}, \quad (\text{A2})$$

where we have slightly modified the notation of Ref. [29].³

More symmetric phases are contained in this parametrization as special cases:

In the non-superconducting phase all anomalous self-energy components vanish, $\phi_i^+ = 0$, and the normal self-energy is diagonal in color and flavor, *i.e.*, $\Sigma_i^+ = 0$ for $i = 2, 4, 5$. The remaining self-energy components are equal for up and down quarks, but can be different for strange quarks, *i.e.*, $\Sigma_1^+ = \Sigma_7^+$ and $\Sigma_3^+ = \Sigma_6^+$.

In the 2SC phase, only red and green up and down quarks are paired, described by $\phi_1^+ = -\phi_2^+$, whereas all other components of the anomalous self-energy vanish. Accordingly, the normal self-energy depends on whether it corresponds to paired (red or green) up or down quarks (Σ_1^+), unpaired (blue) up or down quarks (Σ_7^+), or to strange quarks ($\Sigma_3^+ = \Sigma_6^+$), while the non-diagonal components vanish again.

In the CFL phase with three massless flavors, the residual symmetry is $SU_{c+V}(3)$, generated by $\tau_a - \lambda_a^T$ with $a = 1, \dots, 8$, and the quasi-particle spectrum consists of an octet and a singlet [17]. Therefore there are only two independent color-flavor components of the anomalous self-energy [58], $\phi_1^+ = \phi_6^+ = \phi_7^+$, $\phi_2^+ = \phi_4^+ = \phi_5^+$, and $\phi_3^+ = \phi_1^+ + \phi_2^+$. Analogous relations hold for the normal self-energies.

Appendix B: A remark on the iterative procedure

Throughout this work we use a fixed point iteration to obtain the self-consistent solutions of the DSE. Schematically, this can be formulated as an iteration

$$x_{i+1} = \varphi(x_i) \quad (\text{B1})$$

with the fixed points $x^* = \varphi(x^*)$, which correspond to the solutions of the DSE.

In general, however, not every solution can be found in this way, but the iteration only converges if it is contracting, *i.e.*, if

$$\frac{|x_{i+1} - x^*|}{|x_i - x^*|} = \frac{|\varphi(x_i) - \varphi(x^*)|}{|x_i - x^*|} \stackrel{!}{\leq} L \quad (\text{B2})$$

³ Our P_6 and M_6 correspond to P_7 and M_7 in Ref. [29] and our P_7 and M_7 correspond to P_8 and M_8 , while there are no projectors P_6 and M_6 in that reference.

with a constant $L < 1$. This expression is just the discretized derivative $|\varphi'(x^*)|$.

The phase diagrams and in particular the spinodal lines presented in Sec. V are based on the assumption that the numerically stable solutions of the DSE, *i.e.*, those solutions for which the iteration converges, also correspond to thermodynamically stable or metastable solutions, *i.e.*, to global or local minima of the thermodynamic potential.

This conjecture is motivated by the observation that it holds in the NJL model, where it can be shown analytically. To this end, we consider the standard NJL model, defined by the Lagrangian [59]

$$\mathcal{L}_{NJL} = \bar{\psi}(i\not{\partial} - m)\psi + G [(\bar{\psi}\psi)^2 + (\bar{\psi}i\gamma_5\vec{\tau}\psi)^2] \quad (\text{B3})$$

with bare quark mass m and a positive four-point coupling constant G . The NJL mean-field thermodynamic potential in vacuum is given by (see, *e.g.*, Ref. [14])

$$\Omega = \frac{(M - m)^2}{4G} - 2N_c N_f \int \frac{d^3q}{(2\pi)^3} \sqrt{\vec{q}^2 + M^2}, \quad (\text{B4})$$

which depends on the dressed quark mass M . Additionally a regularization needs to be specified, as the integral is divergent.

The actual value of M is determined by minimizing Ω . This leads to the stationarity condition

$$\frac{\delta\Omega}{\delta M} = \frac{M - \varphi(M)}{2G} \stackrel{!}{=} 0 \quad (\text{B5})$$

with

$$\varphi(M) = m + 4GN_c N_f \int \frac{d^3q}{(2\pi)^3} \frac{M}{\sqrt{\vec{q}^2 + M^2}}. \quad (\text{B6})$$

Obviously, eq. (B5) is equivalent to the DSE (“gap equation”) $M = \varphi(M)$, which has the solutions M^* . The physical stability of these solutions can then be checked by investigating the second derivative

$$\frac{\delta^2\Omega}{\delta M^2} \Big|_{M=M^*} = \frac{1}{2G} (1 - \varphi'(M^*)) \quad (\text{B7})$$

with $\varphi'(M) = \frac{d\varphi(M)}{dM}$. This means, the solution corresponds to a minimum if $\varphi'(M^*) < 1$ and to a maximum if $\varphi'(M^*) > 1$.

Taking the derivative of eq. (B6), one obtains

$$\varphi'(M) = 4GN_c N_f \int \frac{d^3q}{(2\pi)^3} \frac{\vec{q}^2}{(\vec{q}^2 + M^2)^{3/2}} \quad (\text{B8})$$

which is positive for all values of M . Therefore, we have

$$|\varphi'(M^*)| \begin{cases} < 1 & \text{for a minimum of } \Omega \\ > 1 & \text{for a maximum of } \Omega \end{cases} \quad (\text{B9})$$

Comparing this with eq. (B2), we see immediately that the maxima of the potential correspond to numerical unstable iterative solutions, while minima are numerically

stable. This allows in principle to find all minima of the potential by iterating the gap equation. It can also be checked easily that the introduction of finite temperature and chemical potential does not change these results.

For QCD DSEs, the situation is much more compli-

cated as we have functional derivatives and an in principle infinite dimensional system. Therefore we are not able to provide an analogous analytic argument for the relation between physical and numerical stability. However, we expect this relation still to be valid.

-
- [1] P. Braun-Munzinger and J. Wambach, Reviews of Modern Physics **81**, 1031 (2009).
 - [2] K. Fukushima and T. Hatsuda, Reports on Progress in Physics **74**, 014001 (2011), [arXiv:1005.4814 \[hep-ph\]](#).
 - [3] A. Bazavov *et al.*, Phys. Rev. D **85**, 054503 (2012), [arXiv:1111.1710 \[hep-lat\]](#).
 - [4] S. Borsányi *et al.*, Journal of High Energy Physics **9**, 73 (2010), [arXiv:1005.3508 \[hep-lat\]](#).
 - [5] P. de Forcrand and O. Philipsen, Physical Review Letters **105**, 152001 (2010), [arXiv:1004.3144 \[hep-lat\]](#).
 - [6] G. Endrődi, Z. Fodor, S. D. Katz, Szabó, and K. K., Journal of High Energy Physics **4**, 1 (2011), [arXiv:1102.1356 \[hep-lat\]](#).
 - [7] O. Kaczmarek *et al.*, Phys. Rev. D **83**, 014504 (2011), [arXiv:1011.3130 \[hep-lat\]](#).
 - [8] F. Karsch, B.-J. Schaefer, M. Wagner, and J. Wambach, Physics Letters B **698**, 256 (2011), [arXiv:1009.5211 \[hep-ph\]](#).
 - [9] S. Borsányi *et al.*, Journal of High Energy Physics **8**, 53 (2012), [arXiv:1204.6710 \[hep-lat\]](#).
 - [10] K. Rajagopal and F. Wilczek, The Condensed Matter Physics of QCD, in *At the frontier of particle physics, vol. 3*, edited by M. Shifman, pp. 2061–2151, World Scientific, Singapore, 2001, [arXiv:hep-ph/0011333](#).
 - [11] M. Alford, Annual Review of Nuclear and Particle Science **51**, 131 (2001), [arXiv:hep-ph/0102047](#).
 - [12] T. Schäfer, Proc. of the BARC workshop on Quarks and Mesons, Mumbai (2003), [arXiv:hep-ph/0304281](#).
 - [13] D. H. Rischke, Progress in Particle and Nuclear Physics **52**, 197 (2004), [arXiv:nucl-th/0305030](#).
 - [14] M. Buballa, Phys. Rep. **407**, 205 (2005), [arXiv:hep-ph/0402234](#).
 - [15] I. A. Shovkovy, Foundations of Physics **35**, 1309 (2005), [arXiv:nucl-th/0410091](#).
 - [16] M. G. Alford, A. Schmitt, K. Rajagopal, and T. Schäfer, Reviews of Modern Physics **80**, 1455 (2008), [arXiv:0709.4635 \[hep-ph\]](#).
 - [17] M. Alford, K. Rajagopal, and F. Wilczek, Nuclear Physics B **537**, 443 (1999), [arXiv:hep-ph/9804403](#).
 - [18] T. Schäfer, Nuclear Physics B **575**, 269 (2000), [arXiv:hep-ph/9909574](#).
 - [19] I. A. Shovkovy and L. C. R. Wijewardhana, Physics Letters B **470**, 189 (1999), [arXiv:hep-ph/9910225](#).
 - [20] M. Buballa and M. Oertel, Nuclear Physics A **703**, 770 (2002), [arXiv:hep-ph/0109095](#).
 - [21] H. Abuki and T. Kunihiro, Nuclear Physics A **768**, 118 (2006), [arXiv:hep-ph/0509172](#).
 - [22] S. B. Rüster, V. Werth, M. Buballa, I. A. Shovkovy, and D. H. Rischke, Phase Diagram of Neutral Quark Matter at Moderate Densities, in *Pairing in Fermionic Systems: Basic Concepts and Modern Applications*, edited by A. Sedrakian, J. W. Clark, and M. Alford, p. 63, World Scientific Publishing Co, 2006.
 - [23] D. Blaschke, S. Fredriksson, H. Grigorian, A. M. Öztaş, and F. Sandin, Phys. Rev. D **72**, 065020 (2005), [arXiv:hep-ph/0503194](#).
 - [24] C. S. Fischer and J. A. Müller, Phys. Rev. D **80**, 074029 (2009), [arXiv:0908.0007 \[hep-ph\]](#).
 - [25] C. S. Fischer, A. Maas, and J. A. Müller, European Physical Journal C **68**, 165 (2010), [arXiv:1003.1960 \[hep-ph\]](#).
 - [26] C. S. Fischer, J. Lückner, and J. A. Müller, Physics Letters B **702**, 438 (2011), [arXiv:1104.1564 \[hep-ph\]](#).
 - [27] C. S. Fischer and J. Lückner, Physics Letters B **718**, 1036 (2013), [arXiv:1206.5191 \[hep-ph\]](#).
 - [28] D. Nickel, J. Wambach, and R. Alkofer, Phys. Rev. D **73**, 114028 (2006), [arXiv:hep-ph/0603163](#).
 - [29] D. Nickel, R. Alkofer, and J. Wambach, Phys. Rev. D **74**, 114015 (2006), [arXiv:hep-ph/0609198](#).
 - [30] D. Nickel, R. Alkofer, and J. Wambach, Phys. Rev. D **77**, 114010 (2008), [arXiv:0802.3187 \[hep-ph\]](#).
 - [31] Y. Nambu, Physical Review **117**, 648 (1960).
 - [32] L. P. Gorkov, JETP **36(9)**, 1364 (1959).
 - [33] R. D. Pisarski and D. H. Rischke, Phys. Rev. D **60**, 094013 (1999), [arXiv:nucl-th/9903023](#).
 - [34] J. S. Ball and T.-W. Chiu, Phys. Rev. D **22**, 2542 (1980).
 - [35] A. Maas, J. Wambach, B. Grüter, and R. Alkofer, European Physical Journal C **37**, 335 (2004), [arXiv:hep-ph/0408074](#).
 - [36] A. Maas, J. Wambach, and R. Alkofer, European Physical Journal C **42**, 93 (2005), [arXiv:hep-ph/0504019](#).
 - [37] A. Cucchieri, A. Maas, and T. Mendes, Phys. Rev. D **75**, 076003 (2007), [arXiv:hep-lat/0702022](#).
 - [38] M. Le Bellac, *Thermal Field Theory* (Cambridge University Press, 2000).
 - [39] D. Müller, M. Buballa, and J. Wambach, in preparation.
 - [40] J. Beringer and et al., Phys. Rev. D **86**, 010001 (2012).
 - [41] Budapest-Marseille-Wuppertal Collaboration *et al.*, Physics Letters B **701**, 265 (2011), [arXiv:1011.2403 \[hep-lat\]](#).
 - [42] K. G. Chetyrkin and A. Retey, Nuclear Physics B **583**, 3 (2000), [arXiv:hep-ph/9910332](#).
 - [43] R. Williams, C. S. Fischer, and M. R. Pennington, [arXiv:0704.2296 \[hep-ph\]](#) (2007), [arXiv:0704.2296 \[hep-ph\]](#).
 - [44] H. Pagels and S. Stokar, Phys. Rev. D **20**, 2947 (1979).
 - [45] C. D. Roberts and A. G. Williams, Progress in Particle and Nuclear Physics **33**, 477 (1994), [arXiv:hep-ph/9403224](#).
 - [46] J. Skullerud, A. Ki Izlersü, and A. G. Williams, Nuclear Physics B Proceedings Supplements **106**, 841 (2001).
 - [47] R. Alkofer, C. S. Fischer, F. J. Llanes-Estrada, and K. Schwenzer, Annals of Physics **324**, 106 (2009), [arXiv:0804.3042 \[hep-ph\]](#).
 - [48] C. S. Fischer and R. Williams, Physical Review Letters **103**, 122001 (2009), [arXiv:0905.2291 \[hep-ph\]](#).
 - [49] M. Hopfer, A. Windisch, and R. Alkofer, PoS Confine-

- ment X , 073 (2013), [arXiv:1301.3672](#) [hep-ph].
- [50] M. Alford and K. Rajagopal, Journal of High Energy Physics **6**, 31 (2002), [arXiv:hep-ph/0204001](#).
 - [51] D. Nickel, Phys. Rev. D **80**, 074025 (2009), [arXiv:0906.5295](#) [hep-ph].
 - [52] W. Broniowski, Acta Phys.Polon.Supp. **5**, 631 (2012), [arXiv:1110.4063](#) [nucl-th].
 - [53] D. V. Deryagin, D. Y. Grigoriev, and V. A. Rubakov, International Journal of Modern Physics A **7**, 659 (1992).
 - [54] E. Shuster and D. T. Son, Nuclear Physics B **573**, 434 (2000), [arXiv:hep-ph/9905448](#).
 - [55] J. A. Bowers and K. Rajagopal, Phys. Rev. D **66**, 065002 (2002), [arXiv:hep-ph/0204079](#).
 - [56] R. Casalbuoni and G. Nardulli, Reviews of Modern Physics **76**, 263 (2004), [arXiv:hep-ph/0305069](#).
 - [57] R. Anglani *et al.*, [arXiv:1302.4264](#) [hep-ph] (2013), [arXiv:1302.4264](#) [hep-ph].
 - [58] M. Alford, J. Berges, and K. Rajagopal, Nuclear Physics B **558**, 219 (1999), [arXiv:hep-ph/9903502](#).
 - [59] Y. Nambu and G. Jona-Lasinio, Physical Review **124**, 246 (1961).